Using Ray Tracing to Improve Bridge Monitoring With High-Resolution SAR Satellite Imagery

Zahra Sadeghi , Tim Wright , Andrew Hooper , *Senior Member, IEEE*,
and Sivasakthy Selvakumaran , *Member, IEEE*

Abstract—While satellite persistent scatterer synthetic aperture radar (SAR) interferometry is an effective technique to monitor the health of structures via selection of long-term coherent pixels, detailed interpretation of displacement measurements requires knowledge of which surfaces, the reflection is coming from. Ray tracing algorithms can be used to simulate SAR backscatter for structures, and link observed PS pixels to specific parts of structures. We investigate the reflectivity of three bridges in London for a high-resolution TerraSAR-X dataset, using a ray tracing technique. Artificial reflectors are mounted on one of the bridges. We compare the simulated backscatter with the location of points selected as PS pixels using a stack of 38 TerraSAR-X images. The results confirm that we can predict overall scattering behavior of a bridge using SAR simulation techniques when we have access to a 3-D model of the structure. However, the results of simulation depend on the level of details in the 3-D model and a high-detailed 3-D model including corner reflectors allows the ray tracing technique to perfectly simulate position of the strong scatterers. This approach can help designers increase the SAR reflectivity of a bridge in the design phase of structural bridge assets, or in a retrofit phase, by installing artificial reflectors. We also link the strong scatterers in the reflectivity map to the corresponding scattering surfaces in the structural model that contributed to the signal. This allows the end-users of the InSAR products to better understand which sections of a bridge are moving when a PS pixel indicates displacement.

Index Terms—Bridge health monitoring, Persistent scatterer SAR interferometry (PSInSAR), ray tracing.

I. INTRODUCTION

THERE is a growing need to monitor a portfolio of ageing structures globally. The primary method for monitoring structures currently is periodic visual inspection, but the damage

and collapse in recent years of several high profile structures highlights the limitations and challenges of this method [1]. More detailed inspection methods such as surveying and instrumentation of sensors provide quantified measurements but are limited in terms of access and scalability.

Generally, these methods for structural stability monitoring are expensive as they are reliant on time-consuming surveys, various surveying instruments, and surveying resources. Satellite synthetic aperture radar interferometry (InSAR) techniques have the potential to monitor the behavior of structures over a wide geographic area with a regular frequency (every few days), at relatively low cost [2]. InSAR can monitor assets which are difficult to access more frequently for inspection or assets in hazardous areas. By taking advantage of archived satellite imagery, InSAR can also be used to look back in time and assist in baseline studies prior to construction with the possibility of identifying unstable areas [3].

Various InSAR time-series approaches have been developed to extract maximum displacement information from noisy InSAR interferograms [4], [5]. Persistent scatterer InSAR (PSI) methods [6], [7], [8], [9] were presented to identify points (persistent scatterers or PS) that show coherent scattering behavior over large temporal baselines, when many pixels become incoherent in conventional InSAR. The stanford method for persistent scatterers (StaMPS) improved the number of PS in rural areas and removed the linear displacement model implicit in original PS algorithms [10]. In these techniques, a large range of perpendicular baselines in individual interferograms is used and only persistent dominant point scatterers, which are single reflectors inside each cell, remain coherent.

Some satellite missions, such as TerraSAR-X and Cosmo-SkyMed, collect synthetic aperture radar (SAR) images with sufficiently high spatial resolutions (in the order of a few meters or less) such that InSAR can provide a sufficiently high density of measurement points to allow structural health monitoring of different sections of a desired structure [11], [12]. In the last decade, large numbers of applications of InSAR techniques including PSI were presented for stability monitoring of tunnels, railways and highways [13], [14], [15], [16], [17], dams [18], [19], bridges [20], [21], [22], [23], [24] and cities [25] using high resolution SAR data sets. InSAR can be combined with other geodetic measurements e.g., Lidar, ground penetrating radar (GPR) and Global Navigation Satellite System (GNSS) to provide more robust stability monitoring data over individual structures [26], [27], [28], [29]. A combination of InSAR data

and Markov chain Monte Carlo approach for assessing a single structure deformations was also presented by Milillo et al. [22] to solve for 3-D displacements and their relative errors. On a large scale, Chang et al. [14] presented a probabilistic method for InSAR time-series postprocessing to estimate the most probable displacement parameters for each InSAR PS point in order to set up a nationwide systematic railway monitoring system.

Side-looking SAR sensors create a challenge for interpreting features of structures, such as bridges in SAR images. Radar image distortions, such as layover and shadow are sources of some of these effects. The challenge also includes finding where back-scattered signal comes from and how the SAR image features relate to the real features on the ground. Multiple-bounce effects can also create difficulty where the back-scattered signal interacts with more than one scattering surface on the ground. Soergel et al. [30] used multiple-bounce effects for a bridge spanning above the water to estimate its height. Qin et al. [24] defined how the different components of the bridge contribute to the signal of PS pixels in the results of PSI analysis. Most of the bridges have steel structures that expand and contract with temperature, therefore thermal dilations make a challenge to be separated from the bridge displacement term. Monserrat et al. [23] proposed an accurate approach to model thermal dilation displacements of bridges and it explicitly made use of the temperatures at the time of acquisition of the SAR image. Hlaváčová et al. [20] presented a monitoring study for the Radotín bridge using InSAR technique, with different requirements: estimation of thermal dilation only, of linear deformation only and of both together. However, the most reasonable results were found when estimating only the thermal dilations. Selvakumaran et al. [31] also compared thermal expansion component of Hammersmith flyover estimated by PSI analysis and measured by in situ monitoring and the results confirmed an excellent agreements between the two datasets. Weak backscattering signals from some of the bridges due to their surface characteristics is another challenge to monitor them using SAR imagery. Selvakumaran et al. [32] presented a study to design and install synthetic corner reflectors to increase the signal strength from Waterloo bridge in the SAR images.

To maximize the utility of InSAR for monitoring the health of structures, finding the locations of physical scatterers on the structure and surrounding features that correspond to selected InSAR pixels (PS points) is essential for the end-users in the civil engineering community. This can be challenging, as multiple surfaces can interact with the radar signal and contribute to the intensity of the points. Moreover, the scattering characteristics of the structures influence their level of reflectivity in the SAR images; design modifications of structures prior to, or after, construction can help improve their reflectivity. SAR image simulation which simulates the direct backscattering from man-made objects using rendering algorithms can predict the reflectivity in SAR images [33], [34], [35], [36]. Furthermore, ray tracing methods based on SAR simulation are able to trace back each simulated PS candidate to the scattering surfaces on the corresponding structure [37] and provide the required knowledge about the nature of the PS candidates.

The main requirement for SAR image simulation is a 3-D geometrical representation of the desired area that should be realistic. SPECRAY-EM/FERMAT (http://www.oktal-se.fr/), GRECOSAR [38], PIRDIS [39], and RaySAR [37] are SAR simulation methods which: use raytracing methods to simulate radar signals; account for multiple reflections of radar signals; are enable to simulate very high resolution (VHR) SAR data; and simulate detailed object models. RaySAR addressed limitations of the other similar methods by: applying 3-D SAR simulation in azimuth, range and elevation; providing methods for geometrical analysis of scatters; and by linking scatterers in the simulated scene to the geometry of structures. RaySAR keeps track of each individual scatter and provides its corresponding 3-D location and bounce level e.g., double or triple bounce. RaySAR is computationally efficient due to using simplified reflection models, which we discuss in Section II-A.

Auer et al. [40] generated a simulated VHR SAR image (TerrSAR-X Spotlight) using RaySAR with a highly detailed 3-D model of a building in the centre of Berlin. They localized geocoded PSs in 3-D using heights with respect to a reference DEM, and compared them with the 3-D positions of simulated signatures with multiple bounce scattering levels in the coordinates of the building model. They attributed a shortfall in the number of simulated signatures with triple bounce scattering behavior, compared to the detected PS, as due to lack of high-resolution detail in the 3-D model.

Yang et al. [41] also investigated the potential of predicting the location of PS pixels using the RaySAR ray tracing method and found good correspondence between selected PS pixels and point signatures predicted by the SAR simulator. The amount of detail and spatial resolution of a 3-D city model is specified as "level of detail" (LOD). LOD1 is a model in which buildings are represented as blocks. LOD2 is a more detailed model including roof shapes [42]. Yang et al. [41] also investigated the impact of level of detail in the available city model. They found that 10% and 37% of the selected PSs in the TSX processing for a test area could be matched with the potential PS pixels in the simulated results, using LOD1 and LOD2, respectively. They also concluded that using higher LOD models might further increase the fraction of identified scatterers.

The literature reveals that health monitoring of bridges, in particular, has been developing as a topic of interest within the InSAR research field in recent years. In our research, we analyze the ability of PSI to select PS pixels on bridges, and then test modifications that might increase reflectivity (either before built or by adding additional components such as artificial reflectors). We focus on bridges with different reflecting characteristics and 3-D models with various level of details. One of the main goals in this research is to study capability of the RaySAR to simulate reflectivity map for bridges with different characteristics and compare with real reflectivity map using high-resolution TerraSAR-X images. This can help to assess factors impacting on the level of visibility of bridges in the amplitude maps and be helpful for the design consultant to predict and/or improve it before or after construction. Another goal of this article is to find surfaces contributing to the signal of specific selected points using tracing back to 3-D model to better understand the locations of physical scatterers on the structure and surrounding features. As mentioned before, this information cannot be extracted from PSI results and help the InSAR end-users to

link the PSI outputs with the structure's components. We apply StaMPS for PSI processing (see Section II) and compare the selected PS pixels with strong scatterers in the simulated maps. Then, we link the simulated strong scatterers matching with PS pixels to the 3-D model to better understand which scattering surfaces contribute to the signal of each selected pixel. The techniques we explore can inform bridge design to develop designs that include a strategy for future stability monitoring using InSAR satellites. It should be noted that this article does not create new methodological advancements, but it focuses on furthering application of PSI and ray tracing. We introduce our case studies, 3-D models, SAR data sets and data preparation in Section III. We present results of simulation and InSAR processing in Section IV and discuss them in more details. Finally, Section V concludes this article.

II. METHODOLOGY

We used the RaySAR method for SAR simulation via ray tracing [37] and the StaMPS method to select PS pixels and calculate their displacement time series [10]. In this section, we introduce the above methods briefly as follows.

A. RaySAR for SAR Simulation

Ray tracing is a rendering method which traces rays through a 3-D model and simulates the reflections based on their interactions with the surface. RaySAR is a 3-D SAR simulator approach based on the open-source ray tracer POV-Ray (Persistence of Vision Ray Tracer), which has been adapted for a SAR imaging geometry [37]. The SAR system is represented by a camera characterized by orthographic projection in azimuth and elevation as well as by a signal source emitting parallel light. RaySAR represents an ideal SAR system with infinite resolution in azimuth, range and elevation; this means that a corner reflector is focused to a point in 3-D space.

Using RaySAR, we can link the surfaces illuminated by the virtual radar signal to signatures within the simulated image. Signatures in the real SAR image can then be cross-compared to link the SAR image to reflecting surfaces in the 3-D model space.

The RaySAR simulation process include three phases: 3-D scene modeling; model sampling; and reflectivity map production. A 3-D model of the case study needs to be imported to the ray tracer. In order to simulate reflection from medium-sized features i.e., trihedrals with a sidelength of around 10 cm for very high resolution SAR systems in X-band, the resolution of the 3-D model should be sufficiently high to include them. The ray tracer package (POV-Ray) traces rays through the model and analyses the backscattering contributions. It results in a list of sampled points and their intensities for all intersections between the ray and the 3-D model. This irregularly distributed data cloud is then gridded in radar coordinates to generate a simulated reflectivity map.

In order to apply SAR simulation via RaySAR, three main components need to be defined: the geometry of objects; the surface characteristics for all objects; and the positions and parameters of the virtual SAR. The simulated signal depends on
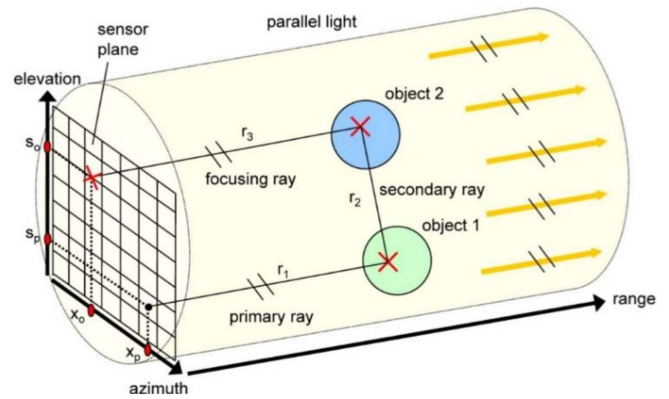

Fig. 1. Schematic representation of raytracing process to localize a double-bounce reflection signal (reproduced with permission from [37]).

the imaging geometry, the combination of diffuse and specular reflectivity coefficients, and weight factors scaling the intensity of multiple reflections. RaySAR models and sums up diffuse and specular intensities for each signal reflection within the 3-D model. The RaySAR model for specular reflection represents each signal by a "specular highlight," which may be interpreted as a combination of a peak in the specular direction, surrounded by diffuse components. For most surfaces in urban areas, the strength of diffuse reflected radar signals depends on the direction of the reflection; for direct backscattering of radar signals, the RaySAR model for diffuse reflection considers the dependence on the reflection direction. However, strong overestimation of the diffuse signal response is expected in the case of multiple reflections. Therefore, as an alternative solution for diffuse reflection estimation, the RaySAR model for specular reflection ("specular highlight") can be used simultaneously for approximating specular and diffuse components of radar backscatter. By choosing a high specular reflection coefficient (S), a strong specular reflection will be defined, and choosing an appropriate value for surface roughness factor (R) controls the distribution of diffuse components. The surface roughness is parametrized by surface standard deviation and surface correlation length [37], [41]). The intensity of multiple reflections is scaled by a weight factor for the specular reflection (W). The values for these parameters are calculated for low roughness and medium roughness surfaces for man-made objects as $S = 0.7$, $W = 0.7$, and $R = 8.5 \times 10-4$ for low roughness surfaces and $S = 0.5$, $W = 0.5$, and $R = 3.3 \times 10-4$ for medium roughness surfaces. The illuminated surface consisting of bare soil in man-made environment including ground surfaces and buildings has a constant relative permittivity of $5.7 + j \cdot 1.3$ in X-band [37].

After definition of the surface parameters, the 3-D object scene is sampled based on pixel centers located in the sensor plane. The positions of pixels in ground range depends on the imaging geometry and they are irregular distributed. For each pixel in the sensor plane, the signal contribution is estimated. Fig. 1 shows a schematic ray tracing of a signal with double bounce reflection in an object scene. A primary ray is generated perpendicular to the image plane of the orthographic sensor at location of a pixel center (x_p, s_p). The ray is followed along
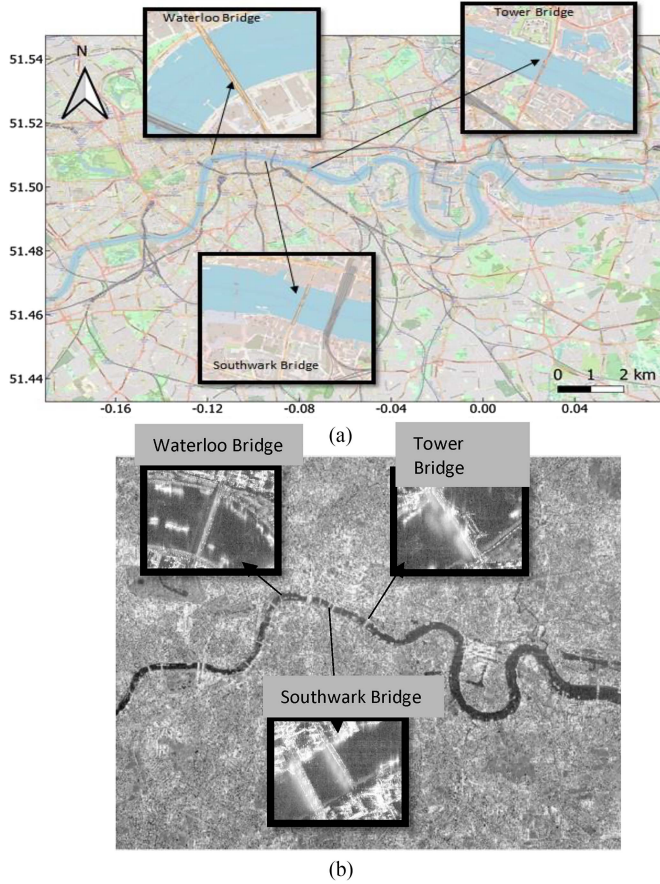
Fig. 2.   (a) Open street map of London. (b) Temporally averaged reflectivity map from 38 TerraSAR-X dataset with zooms of Waterloo bridge, Tower bridge, and Southwark bridge.
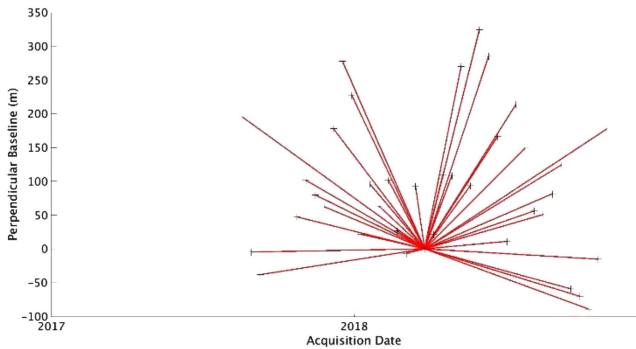

Fig. 3.   Spatial and temporal baseline for 37 TerraSAR-X secondary images with respect to the primary in 20180324.

its path to the object scene where the first intersection point is found.

At the position of the first intersection with an object a secondary ray will point in the specular direction and may intersect with a second object. The amplitude of the signal in the secondary ray direction is weighted using the defined reflection coefficient associated with the first object. A ray parallel to the primary ray (the focusing ray) is created at the second inter-section point, which provides the coordinate of double-bounce
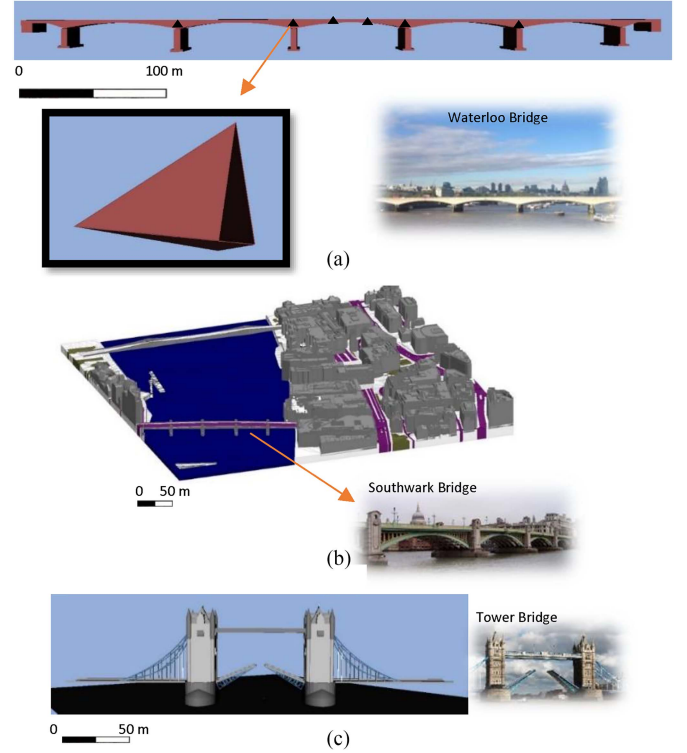

Fig. 4.   3-D models of (a) Waterloo bridge, including installed trihedral corner reflectors. (b) Scene in central london including Southwark bridge. (c) Tower bridge (the models are described in the above paragraphs).

reflection as follows:

$$x_s = \frac{x_p + x_o}{2} \qquad (1)$$

$$r_s = \frac{r_1 + r_2 + r_3}{2} \qquad (2)$$

$$s_s = \frac{s_p + s_o}{2} \qquad (3)$$

where x_s, r_s, and s_s are the position of the scattering center in the azimuth, range and elevation direction. p and o subscripts correspond to the intersection of the sensor plane with the primary and focusing ray, respectively. The ray tracing method (POV-Ray) produces a signal vector for each detected radar signal:

$$S_s = [x_s\; r_s\; s_s\; A_s\; b_s\; f_s\; X_i\; Y_i\; Z_i] \qquad (4)$$

where A_s is the amplitude of the signal, b_s is the corresponding bounce level, which can be up to fivefold, f_s is a flag showing specular reflections (0 for nonspecular, 1 for specular), and X_i, Y_i, and Z_i are coordinates of the detected intersection points.

The output of enhanced POV-Ray is a list of vectors for each scattering center, which is named "contributions." In case of a single bounce, the corresponding signal contribution is defined by a 1×6 vector according to (4). In case of a higher reflection level, such as a triple-bounce, the corresponding signal contribution is defined by a 3×6 matrix.

The extracted signal contributions are irregularly distributed in the azimuth-range plane. In order to produce a reflectivity
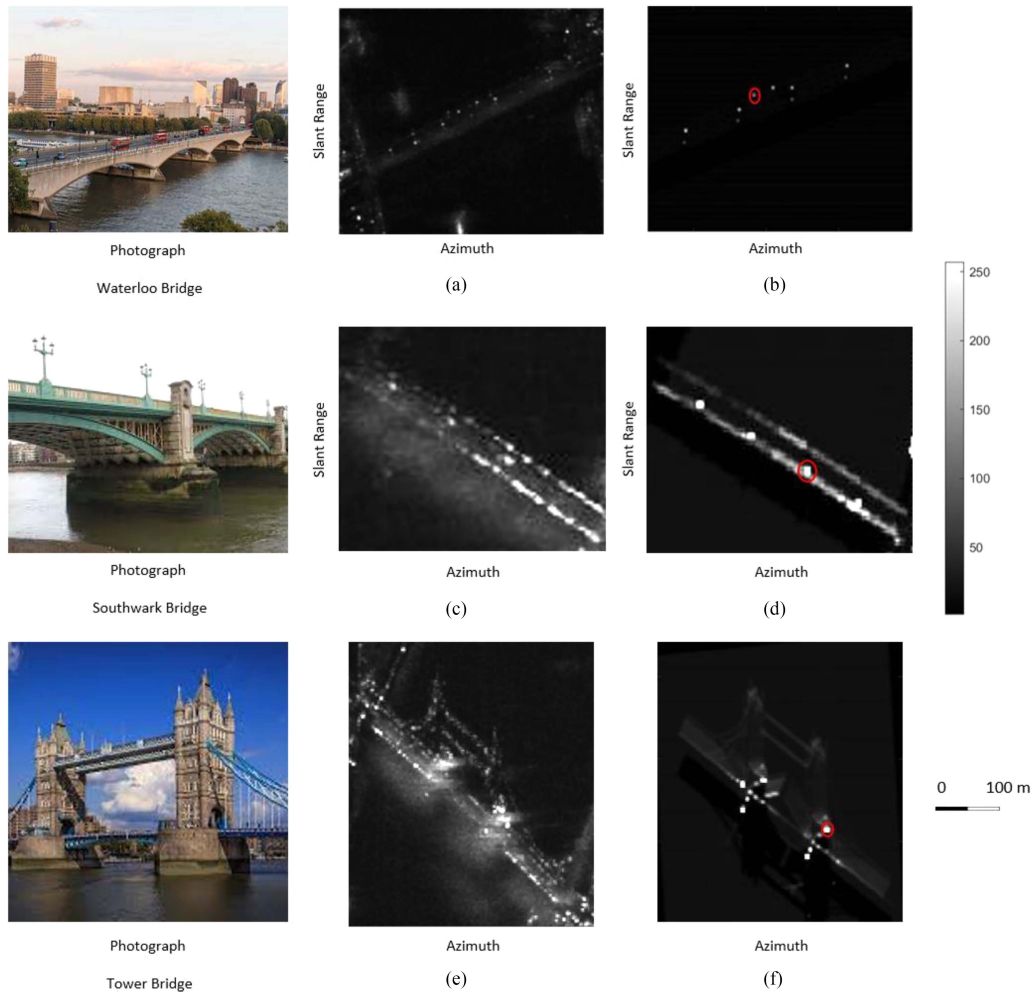
Fig. 5. Temporally averaged reflectivity map from 38 TerraSAR-X dataset for (a) Waterloo bridge, (c) Southwark bridge and (e) Tower bridge. Simulated reflectivity map for (b) Waterloo bridge, (d) Southwark bridge and (f) Tower bridge. The scatterers inside the red circles are traced back in Figs. 9–11.

map, a regular grid is imposed onto the illuminated area, and its resolution in the range and azimuth is defined by the operator. Different contributions are added, either coherently or incoherently, to generate a simulated SAR reflectivity map. Selection of the approach for the contribution summation in this article depends on the level of detail in the 3-D model, which is specified in Section III.

B. StaMPS InSAR for PS Selection

StaMPS is a PSI method that addresses some limitations of conventional PSI approaches for non-urban environments, and for deformation that is erratic in time. The key characteristic of this method is selecting PS pixels based using iterative spatial filtering [10]. Temporal coherence, γ_x, which is a measure of phase noise level and indicator of whether a pixel is a PS, is defined as follows:

$$\gamma_x = \frac{1}{K} \left| \sum_{k=1}^{K} \exp\left\{ i \left(\varphi_{x,k} - \bar{\varphi}_{x,k} - \hat{\varepsilon}_{x,k} \right) \right\} \right| \quad (5)$$

where K is the number of processed interferograms, $\varphi_{x,k}$ is flattened and topographically-corrected interferometric phase,

$\bar{\varphi}_{x,k}$ is spatially filtered phase and $\hat{\varepsilon}_{x,k}$ is an estimate of nonspatially-correlated residual topographic phase. PS candidates are selected using a low amplitude dispersion index threshold. Then, for each PS candidate $\bar{\varphi}_{x,k}$, $\hat{\varepsilon}_{x,k}$, and γ_x are estimated in an iterative process until temporal coherence convergence is achieved.

After selection of PS pixels, the wrapped phases are unwrapped in time and space using a 3-D approach. Finally, the spatially correlated and uncorrelated phase terms that mask the deformation signal are estimated from the unwrapped phase. The deformation signal is subsequently obtained by subtraction of the estimated nuisance terms.

III. DATA AND CASE STUDIES

The diverse structural forms of bridges across the Thames, as well as the availability of regular acquisitions of SAR images, including from high-resolution sensors such as TerraSAR-X, make London an ideal case to study and demonstrate InSAR capabilities to measure stability of man-made features [25]. Therefore, we selected London as our main study area [see Fig. 2(a)]. The TerraSAR-X amplitude map of London [see Fig. 2(b)] shows
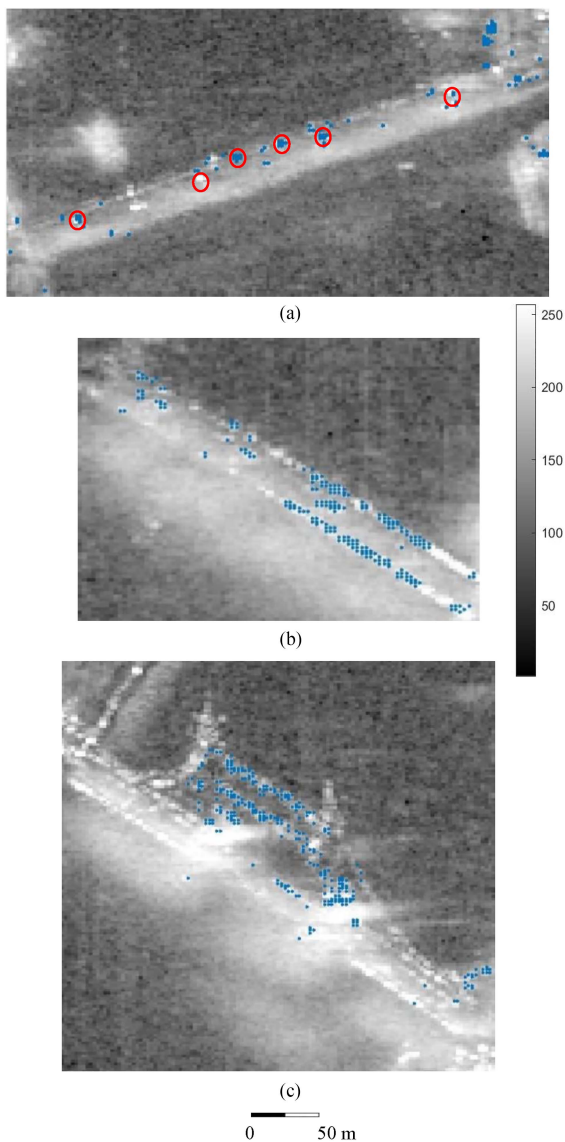
Fig. 6. Selected PS pixels using StaMPS overlaid on average amplitude for (a) Waterloo bridge, (b) Southwark bridge, and (c) Tower bridge. The red outlined circles highlight the locations of the installed corner reflector.

Fig. 7. Geocoded selected PS pixels using StaMPS overlaid on Google satellite map for (a) Waterloo bridge, (b) Southwark bridge and (c) Tower bridge.

different levels of reflectivity for different structures. As case studies, we selected Waterloo bridge, as a concrete structure with poor natural reflectivity and bright installed artificial reflectors, Tower bridge, as a structure with large towers and multiple levels made of steel, concrete and granite with strong reflectivity, and Southwark bridge, as a bright structure made from steel and granite. This allows us to investigate the simulation of structures with different characteristics and reflectivity levels.

Fig. 3 shows the spatial and temporal baselines for the interferograms we formed from 38 TerraSAR-X stripmap images with ascending geometry acquired between August 2017 and November 2018, using a single prime approach. The spatial resolution of the single-look SAR images in the azimuth and slant range directions is 3.3 and 1.17 m, respectively. Waterloo Bridge is a 434 m concrete road bridge which does not show a strong signature in the TerraSAR-X images. To improve radar

reflectivity, six aluminum trihedral corner reflectors [32] with interior edge of 35 (cm) were installed on either side of the bridge. Those installed on the west side of bridge are visible in SAR images acquired by the ascending mode of TerraSAR-X. These corner reflectors create strong and distinguishable point signatures in the amplitude images, which increase visibility of the bridge in the SAR images, and were processed as PS pixels to

Fig. 8. Simulated triple-bounce reflectivity map for waterloo bridge.

Fig. 9. Distribution of signal samples for a 3-D model of the six installed corner reflector.

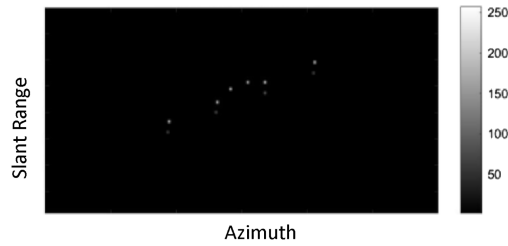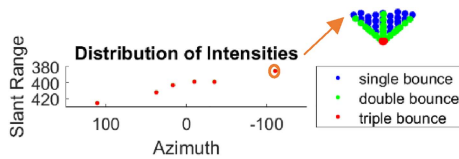monitor their stability [43]. We used our own simple 3-D model of Waterloo Bridge (made using bridge record drawings [44] and added the six trihedral corner reflectors, which we modelled as oriented towards the LOS of TerraSAR-X using Autodesk Revit software [see Fig. 4(a)]. As is clear from the figure, the simple 3-D model of the bridge includes only the basic geometric structures of the bridge. In the 3-D model, the water surface is assumed to be a horizontal plane intersecting the bridge at its lowest height level and we defined low roughness with specular reflection for the water plane. If a detailed 3-D model is available, applying a coherent summation of the signal (which sums up the complex values for different bounce level to map intensity from all reflections) within the RaySAR package improves the similarity of the simulated output to the real case. Conversely, for a low-detailed 3-D model, it is usually not recommended to apply coherent summation. However, we applied coherent summation, as this works best for the corner reflectors. To force a strong backscattering signal from the corner reflectors with respect other features in the model, we defined them with a strong specular reflection and high roughness and assumed low roughness and low specular reflection for the water surface and the bridge layer. This helped to improve the similarity of simulated reflectivity map to the real case when applying coherent summation of the signal.

We also had access to a 3-D model of a small scene in central London covering Southwark Bridge mapped by AccuCities in a 2016 aerial survey data [see Fig. 4(b)].[1] In the 3-D model of the tile in the central London, the water surface (layer) has been defined as a plane intersecting the bridge and riverside at height of −5 m. This bridge model contains three layers: the "road_bridge" layer contains a simple model of the deck of the bridge; the "terrain_bridge" layer contains a simple model of the pedestrian and cycle path and the "wall_bridge" layer contains a simple model of the other structural components including the granite piers and metal parapets (but excluding the steel arches).

[1][Online]. Available: https://www.accucities.com/

The "wall_bridge" layer contains both steel and granite materials, and the "road_bridge" layer and "terrain_bridge_layer" made of asphalt and concrete. We assumed low roughness parameters for the wall_bridge and medium roughness parameters (for both "road_bridge" layer and "terrain_bridge_layer"). For the water surface, we again assumed low roughness with specular reflection. We also used coherent summation approach for this 3-D model.

We also used a detailed 3-D model of the Tower bridge [see Fig. 4(c)] from the Google 3-D warehouse (Google,2011). The 3-D model of Tower bridge includes 17 layers defining different components of the bridge, such as steel hangers, steel suspension chains, north and south main towers (including three different sections), upper footway, deck and tower piers. In the 3-D model of Tower bridge, the water surface is again assumed to be a plane intersecting the bridge at its lowest height level. We assumed low roughness for steel components of the bridge, medium roughness for the rest, and again we assumed low roughness with specular reflection for the water surface. We again applied coherent summation approach for the signal simulation of this detailed 3-D model.

We opened the 3-D models in the AccuTrans3D software and saved them in an acceptable format for the POV-Ray ray tracer (.pov). We edited the 3-D models in POV-Ray software to define the geometry and spatial resolution of the TerraSAR-X data and the simulation parameters for synthesizing the reflectivity values. To define the geometry of our TerraSAR-X data, we introduced the local incidence angle and heading angle to the 3-D model. First, we calculated the local incidence angle for the center of each 3-D model scene using the incidence angle of the four corners of the SAR image, e.g., 37.3° for Waterloo bridge. Then we simulated the position of the SAR satellite looking at the center of the scene with the same local incidence angle. We also transformed the heading angle of the satellite from space to ground plane (353.95°) and input it to the RaySAR package to synthetize the geometry of the satellite.

We defined the pixel spacing of the SAR image in azimuth and slant range direction and sampled the 3-D models using the POV-Ray ray tracer with our defined sampling distance. We defined the sampling rate such that we ensure collecting enough number of signal contribution from the corner reflectors i.e., 5 cm times 5 cm for the Waterloo bridge model and of 0.17×0.17 m for the other 3-D models.

IV. RESULTS

We present results of the SAR simulation (ray tracing) for Waterloo, Southwark, and Tower bridges and compare with the results of PSI from TerraSAR-X data.

A. Waterloo Bridge

The Waterloo bridge 3-D model we used in this article was a challenging case for the simulation in RaySAR because the 3-D model of the bridge was very simple and low in detail, whilst the corner reflectors were modeled separately, creating a high-level detail within the simple model.
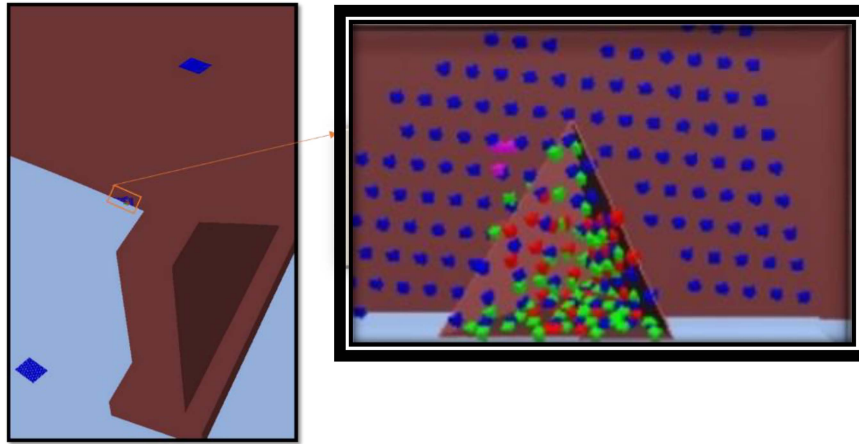
Fig. 10.   Representation of simulated intersection points in the waterloo bridge 3-D model corresponding to the scatterer inside the red dot located in Fig. 5(b). The intersection points are shown with 0.04 and 0.01 m cubes in two different zoom, respectively, where colors indicate the bounce level, blue for single-bounce, green for double-bounce, red for triple-bounce and magenta for fourfold-bounce.
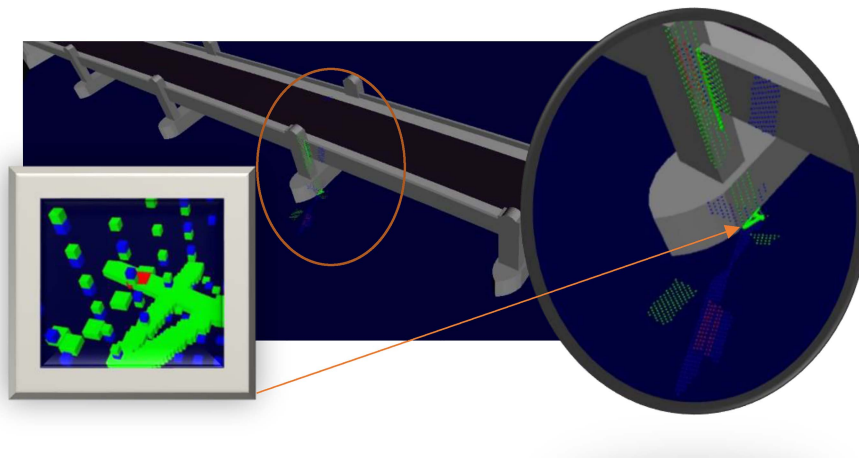

Fig. 11.   Representation of simulated intersection points and phase centers in the southwark bridge 3-D model corresponding to the scatterer inside the red circle in Fig. 5(d). The intersection points and phase centers are shown with 0.04 (m) and 0.01 (m) cubes, respectively, where colors indicate the bounce level, i.e., blue for single-bounce, green for double-bounce and red for triple-bounce.

Fig. 5(a) and (b) shows the real and simulated reflectivity maps for Waterloo bridge. With visual comparison between the simulated and real reflectivity images, we can match the location of strong scatterers in both images e.g., those belonging to the corner reflectors in the Waterloo bridge images. It is clear that there are six similar point signatures, which are related to the corner reflectors. StaMPS selected five of the corner reflectors as PS [see Fig. 6(a)]. The results of simulation are similar to the expected pattern for the corner reflectors, i.e., we have strong triple-bounce reflections (see Fig. 8) and poor single and double-bounce reflections.

Fig. 9 shows the distribution of simulated phase centers in the 2-D azimuth-range plane for each corner reflector and confirms that the triple-bounce signal responses of the corner reflectors are concentrated at the corner tip, and single and double-bounce radar signal occurs due to weak backscattering from the corner surfaces. We plotted the geocoded results of selected PS pixels over Waterloo Bridge extracted from our PSI analysis in Fig. 7(a). It is not possible for an end-user to figure out

which parts of the bridge and surrounding features belong to the selected PS pixel. As it is clear from this plot, there are bunch of selected PS pixels at the west part of the Bridge specifically at the location of installed corner reflectors, but we cannot find the feature's surfaces interacting with the signal. In order to be able to interpret this, we traced the strong scatterer inside the red circle in Fig. 5(b) and found the corresponding intersection points of the radar signal and the 3-D model surface. As is visible in Fig. 10, although most of the intersection points correspond to a corner reflector, there are sections of the bridge surface and water level, which contribute to form a bright signal at the position of the red circle.

B. Southwark Bridge

Fig. 5(c) and (d) shows real and simulated amplitude maps for Southwark Bridge as part of the 3-D scene for central London. The real amplitude map shows that the border of bridge is quite reflective and distinguishable. The comparison of the simulated
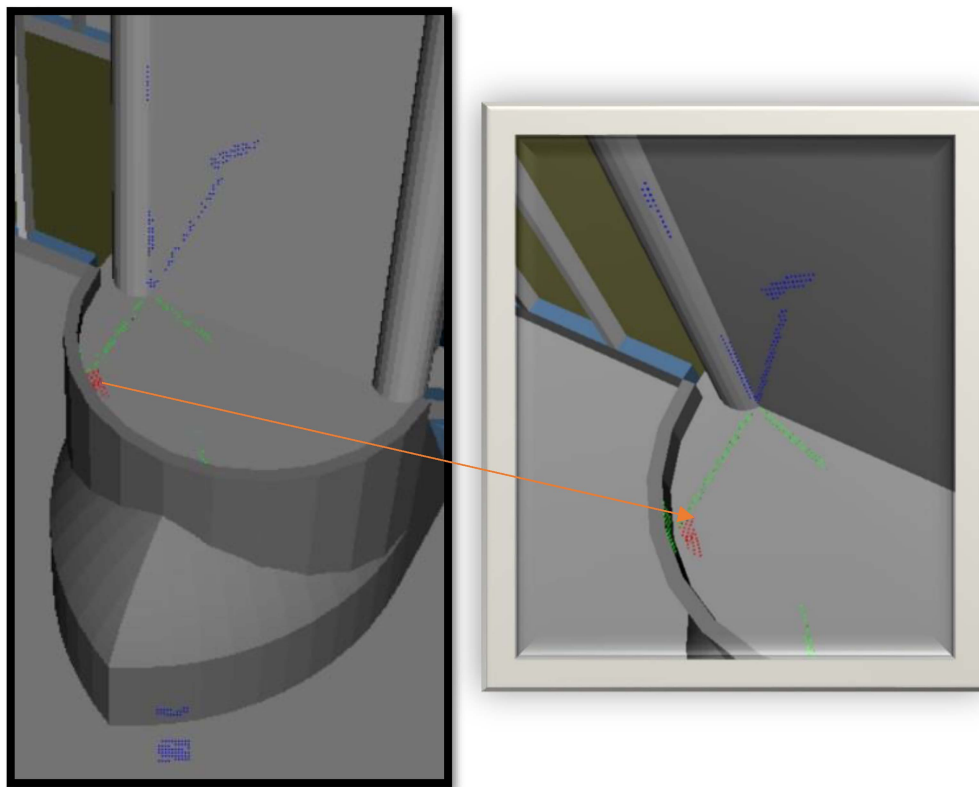
Fig. 12.   Representation of simulated intersection points in the Tower bridge 3-D model corresponding to the point scatterer located inside the red circle in Fig. 5(f). The intersection points are shown with 0.04 (m) and 0.01 (m) cubes, respectively, where colors indicate the bounce level, i.e., blue for single-bounce, green for double-bounce and red for triple-bounce.

and real map confirms that the simulation process worked well. The major similarities between the maps are that: the borders of the bridge are reflective and the bottom-right (north-east) edge of the bridge is the most reflective part. The simulated map shows four strong scatterers at the bottom (eastern) edge, which corresponds to the bridge piers.

Fig. 6(b) shows the PS pixels selected by StaMPS for this bridge, which cluster on the reflective edges. Fig. 7(b) also confirms that the majority of the selected PS pixels are located at the two edges of the Bridge, but it is not possible to figure out whether the signals come from the bridge pier, bridge deck and/or other bridge features at the edge. To better understand which sections of the bridge contribute to the signal of each selected PS pixel, we traced back one of those strong point signatures on the bottom edge of the bridge, inside the red circle in Fig. 5(d), which can be matched with the selected PS pixels in Fig. 6(b).

We found the corresponding intersection points in the object environment which were captured when sampling the 3-D model during raytracing. As is visible in Fig. 11, the location and position of the water surface, bridge deck, bridge piers and bridge base of pier contribute to the selected PS pixels. The selected scatterers show strong triple-bounce and double-bounce reflections and the corresponding intersection surfaces confirm that orthogonal surfaces are the cause. Three orthogonal surfaces can be interpreted as a corner reflector and contribute to a strong triple bounce signal [red circle in Fig. 5(d)].

C. Tower Bridge

The simulated and real reflectivity maps for Tower bridge are plotted in Fig. 5(e) and (f). The level of similarity between the simulated and real map is moderate. In both maps, the general shape of the bridge, suspension chains, north and south main towers and upper footway towers are distinguishable and there are some strong scatterers corresponded to the lower part of the towers. Although Tower bridge is open in the 3-D model, which occurs only when a large ship is passing, it is more realistic than other available 3-D models of the bridges in this research. Moreover, there are 17 different layers in the 3-D model that allowed us to define corresponding simulation parameters for each layer according to its expected (or available) scattering characteristics.

Abundant PS pixels are selected on the bridge, which are mostly clustered on the upper footway and tower sections [see Fig. 6(c)]. Fig. 7(c) plots the geocoded PS points belonging to the Tower bridge. Geocoding errors are visible in this plot due to the low resolution DEM used during PS analysis which doesn't include accurate topography data from the towers. Similar to the Waterloo bridge and Southwark bridge cases, from this plot resulting from a PSI analysis, the end-user cannot find which surfaces in the bridge and towers contribute to the signal of each selected PS pixels. To understand which parts of the bridge can be monitored by selecting pixels by amplitude, we selected one scatterer point highlighted inside the red circle in Fig. 5(f), which can be matched with one selected PS pixels in the real SAR

TABLE I
QUANTITATIVE ASSESSMENT BETWEEN THE SIMULATED AND REAL SAR REFLECTIVITY MAPS

	N_SDB	N_STB	%M_PS1 /SDB	%M_PS2 /STB	%M_PS1 /PS	%M_PS2 /PS
Waterloo	0	6	0	%83	%0	%9
Southwark	18	24	%100	%58	%11	%15
Tower	66	28	%28	%27	%22	%9

image and found the corresponding intersection surfaces/points in the model space (see Fig. 12). This confirms that the selected strong point signatures in the image belong to part of the tower pier, the tower and the water surface, with maximum triple bounce scattering behavior.

V. DISCUSSION AND CONCLUSION

We simulated TerraSAR-X imaging system and corresponding reflectivity maps using RaySAR for Waterloo, Southwark and Tower bridges in London. The results are similar to the real images. This confirms that simple structure 3-D models allow us to predict the key characteristics of the corresponding structures in the SAR images using SAR simulation. However, we showed that SAR simulation is an opportunistic process and the resulting reflectivity map is only as realistic as the input 3-D model.

Adding geometric details to 3-D model of a structure increases the similarity of the simulated image to real SAR image. For a simulation to have real application, a highly-detailed and geometrically accurate 3-D model is required. The impact of the level of geometrical and realistic detail for the 3-D model in the simulation process is visible in the results for the different bridges.

The simulated corner reflectors on Waterloo Bridge, which have more detailed 3-D models compared to other parts of the bridge, are much more similar to the real image. In addition to higher levels of detail, the definition of different layers for each detailed section of a bridge, such as Tower bridge case, improves the simulation as it allows us to define different simulation parameters for each layer based on their characteristics.

An essential part of structural stability monitoring is assessing various elements of the structure, which is typically challenging using InSAR, as the physical origin of identified PS pixels is not understood completely. Finding the relationship between the physical scatterers and PS pixels is key to monitoring the stability of specific components of a structure. A highly-detailed 3-D model of a structure allows us to link the scatterers in the amplitude image to the model and find which scattering surfaces contribute to the signal. This can be helpful to understand the interferometric phase change especially when different sections of a desired structure move in different directions.

Tracing strong scatterers in the simulated images back to the corresponding 3-D models reveals that orthogonal surfaces can generate multiple reflections; three orthogonal surfaces act as a corner reflector and can trigger strong triple bounce reflections that match with PS pixels in the real images. To quantify this, we applied an assessment of relation between corner reflectors traced back from the simulation and selected PS pixels in the real InSAR product. We first identified strong double and triple-bounce scatters in the simulated reflectivity maps that are traced back to the orthogonal surfaces in the 3-D models of the bridges. We assumed that these pixels can be candidates to select as PS pixels. Then, we investigated whether the same scatterers in the real reflectivity map are selected as PS. The results for the three bridges are given in Table I. We defined N_SDB and N_STB as the number of strong double and triple-bounce scatterer that can be traced back to orthogonal surfaces in the 3-D model, respectively. We then found the PS points in the real results matching with the identified N_DBS and S_TBS as M_PS1 and M_PS2 and calculated the ratio of number of M_PS to the N_SDB and N_STB. The %M_PS1/N_SDB and %M_PS1/N_STB can help us to understand what percentage of strong scatterers belonging to orthogonal surfaces are matched with selected real PS. This means how successful would be the simulation to predict PS pixels linking to the strong multiple scatterers. The results show that %83 of N_STB in the Waterloo Bridge are selected as PS in the real results, which is related to the accuracy and details of the 3-D model of the installed corner reflectors. In the Southwark results, %100 of N_SDB and %58 of N_STB are matched with the real PS pixels. These results confirm that most of the predictions of the PS pixels in the simulated data proved to be true for Waterloo and Southwark bridge. On the contrary, simulation for Tower bridge is not as successful as the others, as most of the PS candidates (more than %70) cannot be matched with the real selected PS pixels. Although the similarity between the simulated and real reflectivity map for this bridge is moderate due to the realistic 3-D model with 17 layers of the details, the simulation of multiple scatterers does not match the reality very well. The main reason for this might be defining inaccurate simulation parameters e.g., surface roughness due to lack of knowledge about the material of each part.

Although the simulation process can be successful to predict PS candidates which are selected as PS pixels in the real SAR image, there also might be some real PS pixels which are not simulated as strong multiple-bounce scatterers (PS candidate in the simulated results). Therefore, we also calculated the ratio of M_PS1 and M_PS2 to all selected PS pixels in the real results to measure what percentage of the real PS pixels can be matched with the PS candidates tracing back to orthogonal surfaces in the simulated results. For the all three bridges, these values are less than %22 which means that most of the real PS points were not simulated as strong multiple-bounce signal. The lack of details and geometry's accuracy of the 3-D models and inaccurate surface parameters might be the main reasons for this. Moreover, some PS pixels might be related to

strong single-bounce scatterer which we did not count in our assumption to predict PS candidates in the simulation.

The results of tracing back to the 3-D model also showed that various sections of a bridge (e.g., bridge cross beam surface, bridge pier and pier protection structure) and surrounded objects can contribute to signal of a selected point scatterer in the image.

This article confirmed that the performance of RaySAR method to simulate SAR images is limited to the accuracy of the 3-D model's geometry, level of the details in the 3-D model and knowledge of the surface characteristics parameters. More accurate 3-D model, higher level of details in 3-D model and more information about surface characteristics can improve the simulation process.

The simulation method assists the design consultant to predict radar reflectivity of the structure prior to construction. As expected, our results show that bridges with concrete structures, such as Waterloo bridge are less clear than those that include structural steel elements e.g., Southwark bridge and Tower bridge. Both simulated and real results for Waterloo bridge prove that installing corner reflectors, oriented in the line-of-sight direction, increases the bridge signal in the SAR image significantly and leads to the selection of PS pixels at the location of corner reflectors. Moreover, ability to identify simulated scatterers with strong signal and tracing back them to the 3-D model can help the consultant to predict the locations of PS pixels and find the corresponding surfaces in the 3-D model contributing to the signal of the PS pixels.

ACKNOWLEDGMENT

REFERENCES

[1] S. G. McRobbie, M. A. Wright, and A. Chan, "Can technology improve routine visual bridge inspections?," *Proc. Inst. Civil Eng.-Bridge Eng.*, vol. 168, no. 3, pp. 197–207, 2015.

[2] J. Biggs and T. J. Wright, "How satellite InSAR has grown from opportunistic science to routine monitoring over the last decade," *Nature Commun.*, vol. 11, 2020, Art. no. 3863.

[3] A. Novellino, L. Bateson, and C. Jordan, "Ground motion baseline analysis of the Cheshire U.K. GeoEnergy observatory," *Sci. Rep.*, vol. 11, 2021, Art. no. 15684.

[4] B. Osmanoğlu, F. Sunar, S. Wdowinski, and E. Cabral-Cano, "Time series analysis of InSAR data: Methods and trends," *ISPRS J. Photogramm. Remote Sens.*, vol. 115, pp. 90–102, 2016.

[5] A. Pepe and F. Calò, "A review of interferometric synthetic aperture RADAR (InSAR) multi-track approaches for the retrieval of Earth's surface displacements," *J. Appl. Sci.*, vol. 7, no. 12, 2017, Art. no. 1264.

[6] A. Ferretti, C. Prati, and F. Rocca, "Nonlinear subsidence rate estimation using permanent scatterers in differential SAR interferometry," *IEEE Trans. Geosci. Remote Sens.*, vol. 38, no. 5, pp. 2202–2212, Sep. 2000.

[7] A. Ferretti, C. Prati, and F. Rocca, "Permanent scatterers in SAR interferometry," *IEEE Trans. Geosci. Remote Sens.*, vol. 39, no. 1, pp. 8–20, Jan. 2001.

[8] B. M. Kampes, "Displacement parameter estimation using permanent scatterer interferometry," 2005.

[9] C. Werner, U. Wegmuller, T. Strozzi, and A. Wiesmann, "Interferometric point target analysis for deformation mapping," in *Proc. IEEE Int. Geosci. Remote Sens. Symp.*, 2003, vol. 7, pp. 4362–4364.

[10] A. Hooper, P. Segall, and H. Zebker, "Persistent scatterer interferometric synthetic aperture radar for crustal deformation analysis, with application to Volcán Alcedo, Galápagos," *J. Geophys. Res., Solid Earth*, vol. 112, no. B7, pp. 1–19, 2007.

[11] M. Crosetto, O. Monserrat, R. Iglesias, and B. Crippa, "Persistent scatterer interferometry: Potential, limits and initial C- and X-band comparison," *Photogramm. Eng. Remote Sens.*, vol. 76, no. 9, pp. 1061–1069, 2010.

[12] E. Sansosti et al., "How second generation SAR systems are impacting the analysis of ground deformation," *Int. J. Appl. Earth Observ. Geoinf.*, vol. 28, pp. 1–11, 2014.

[13] G. Barla, A. Tamburini, S. Del Conte, and C. Giannico, "InSAR monitoring of tunnel induced ground movements," *Geomechanics Tunnelling*, vol. 9, no. 1, pp. 15–22, 2016.

[14] L. Chang, R. P. B. J. Dollevoet, and R. F. Hanssen, "Nationwide railway monitoring using satellite SAR interferometry," *IEEE J. Sel. Topics Appl. Earth Observ. Remote Sens.*, vol. 10, no. 2, pp. 596–604, Feb. 2017.

[15] G. Giardina, P. Milillo, M. J. DeJong, D. Perissin, and G. Milillo, "Evaluation of InSAR monitoring data for post-tunnelling settlement damage assessment," *Struct. Control Health Monit.*, vol. 26, no. 2, 2018, Art. no. e2285.

[16] P. Milillo, G. Giardina, M. J. DeJong, D. Perissin, and G. Milillo, "Multi-temporal InSAR structural damage assessment: The London crossrail case study," *Remote Sens.*, vol. 10, no. 2, 2018, Art. no. 287.

[17] D. Perissin, Z. Wang, and H. Lin, "Shanghai subway tunnels and highways monitoring through Cosmo-SkyMed Persistent Scatterers," *ISPRS J. Photogramm. Remote Sens.*, vol. 73, no. C, pp. 58–67, 2012.

[18] P. Milillo et al., "Monitoring dam structural health from space: Insights from novel InSAR techniques and multi-parametric modeling applied to the Pertusillo dam Basilicata, Italy," *Int. J. Appl. Earth Observ. Geoinf.*, vol. 52, 2016, Art. no. 221.

[19] J. J. Sousa et al., "Potential of multi-temporal InSAR techniques for bridges and dams monitoring," *Procedia Technol.*, vol. 16, no. C, pp. 834–841, 2014.

[20] I. Hlaváčová, J. Kolomazník, and L. Halounová, "TerraSAR-X staring spotlight monitoring of a highway bridge in the Czech Republic (preliminary results)," 2015.

[21] M. Lazecky, I. Hlavacova, M. Bakon, J. J. Sousa, D. Perissin, and G. Patricio, "Bridge displacements monitoring using space-borne X-band SAR Interferometry," *IEEE J. Sel. Topics Appl. Earth Observ. Remote Sens.*, vol. 10, no. 1, pp. 205–210, Jan. 2017.

[22] P. Milillo, G. Giardina, D. Perissin, G. Milillo, A. Coletta, and C. Terranova, "Pre-collapse space geodetic observations of critical infrastructure: The Morandi Bridge, Genoa, Italy," *Remote Sens.*, vol. 11, 2019, Art. no. 1403.

[23] O. Monserrat, M. Crosetto, M. Cuevas-González, and B. Crippa, "The thermal expansion component of persistent scatterer interferometry observations," *IEEE Geosci. Remote Sens. Lett.*, vol. 8, no. 5, pp. 864–868, Sep. 2011.

[24] X. Qin, M. Liao, M. Yang, and L. Zhang, "Monitoring structure health of urban bridges with advanced multi-temporal InSAR analysis," *Ann. GIS*, vol. 23, no. 4, pp. 293–302, 2017.

[25] C. A. Bischoff, R. C. Ghail, P. J. Mason, A. Ferretti, and J. A. Davis, "Revealing millimetre-scale ground movements in London using SqueeSAR^{TM}," *Quart. J. Eng. Geol. Hydrogeol.*, vol. 53, pp. 3–11, 2019.

[26] A. M. Alani, F. Tosti, L. B. Ciampoli, V. Gagliardi, and A. Benedetto, "An integrated investigative approach in health monitoring of masonry arch bridges using GPR and InSAR technologies," *NDT E Int.*, vol. 115, 2020, Art. no. 102288.

[27] F. D'Amico, V. Gagliardi, L. B. Ciampoli, and F. Tosti, "Integration of InSAR and GPR techniques for monitoring transition areas in railway bridges," *NDT E Int.*, vol. 115, 2020, Art. no. 102291.

[28] F. Hu, F. J. V. Leijen, L. Chang, J. Wu, and R. F. Hanssen, "Monitoring deformation along railway systems combining multi-temporal InSAR and LiDAR data," *Remote Sens.*, vol. 11, no. 19, 2019, Art. no. 2298.

[29] A. Nahli, E. Simonetto, M. Tatin, S. Durand, L. Morel, and V. Lamour, "On the combination of PsInSAR and GNSS techniques for long-term bridge monitoring," *Int. Arch. Photogramm., Remote Sens. Spatial Inf. Sci.*, vol. 43, pp. 325–332, 2020.

[30] U. Soergel, E. Cardario, A. Thiele, and U. Thoennessen, "Feature extraction and visualization of bridges over water from high-resolution InSAR data and one orthophoto," *IEEE J. Sel. Topics Appl. Earth Observ. Remote Sens.*, vol. 1, no. 2, pp. 147–153, Jun. 2008.

[31] S. Selvakumaran, Z. Sadeghi, M. Collings, C. Rossi, T. Wright, and A. Hooper, "Comparison of in situ and interferometric synthetic aperture radar monitoring to assess bridge thermal expanstion," *Proc. Inst. Civil Eng.-Smart Infrastruct. Construction*, vol. 175, no. 2, pp. 73–91, 2022.

[32] S. Selvakumaran et al., "Combined InSAR and terrestrial structural monitoring of bridges," *IEEE Trans. Geosci. Remote Sens.*, vol. 58, no. 10, pp. 7141–7153, Oct. 2020.

[33] R. Bolter and F. Leberl, "Detection and reconstruction of buildings from multiple view interferometric SAR data," in *Proc. IEEE Int. Geosci. Remote Sens. Symp.*, 2000, vol. 2, pp. 749–751.

[34] J.-M. Nasr and D. Vidal-Madjar, "Image simulation of geometric targets for spaceborne synthetic aperture radar," *IEEE Trans. Geosci. Remote Sens.*, vol. 29, no. 6, pp. 986–996, Nov. 1991.

[35] M. Wohlers, S. Hsiao, J. Mendelsohn, and G. Gardner, "Computer simulation of synthetic aperture radar images of three-dimensional objects," *IEEE Trans. Aerosp. Electron. Syst.*, vol. AES-16, no. 3, pp. 258–271, May 1980.

[36] F. Xu and Y.-Q. Jin, "Imaging simulation of polarimetric SAR for a comprehensive terrain scene using the mapping and projection algorithm," *IEEE Trans. Geosci. Remote Sens.*, vol. 44, no. 11, pp. 3219–3234, Nov. 2006.

[37] S. Auer, S. Hinz, and R. Bamler, "Ray-tracing simulation techniques for understanding high-resolution SAR images," *IEEE Trans. Geosci. Remote Sens.*, vol. 48, no. 3, pp. 1445–1456, Mar. 2010.

[38] G. Margarit, J. J. Mallorqui, J. M. Rius, and J. Sanz-Marcos, "On the usage of GRECOSAR, an orbital polarimetric SAR simulator of complex targets, to vessel classification studies," *IEEE Trans. Geosci. Remote Sens.*, vol. 44, no. 12, pp. 3517–3526, Dec. 2006.

[39] J. Meyer-Hilberg, "PIRDIS: A new versatile tool for SAR/MTI systems simulation," in *Proc. 6th Eur. Conf. Synthetic Aperture Radar*, 2006.

[40] S. Auer, S. Gernhardt, and R. Bamler, "Ghost persistent scatterers related to multiple signal reflections," *IEEE Geosci. Remote Sens. Lett.*, vol. 8, no. 5, pp. 919–923, Sep. 2011.

[41] M. Yang, P. López-Dekker, P. Dheenathayalan, F. Biljecki, M. Liao, and R. F. Hanssen, "Linking persistent scatterers to the built environment using ray tracing on urban models," *IEEE Trans. Geosci. Remote Sens.*, vol. 57, no. 8, pp. 5764–5776, Aug. 2019.

[42] F. Biljecki, H. Ledoux, J. Stoter, and J. Zhao, "Formalisation of the level of detail in 3D city modelling," *Comput., Environ. Urban Syst.*, vol. 48, pp. 1–15, 2014.

[43] S. Selvakumaran, S. Plank, C. Geiß, C. Rossi, and C. Middleton, "Remote monitoring to predict bridge scour failure using interferometric Synthetic Aperture Radar (InSAR) stacking techniques," *Int. J. Appl. Earth Observ. Geoinf.*, vol. 73, pp. 463–470, 2018.

[44] E. J. Buckton and J. Cuerel, "The new waterloo bridge," *J. Inst. Civil Engineers*, vol. 20, no. 7, pp. 145–178, 1943.

Tim Wright received the Ph.D. degree in geophysics/InSAR from the University of Oxford, Oxford, U.K., in 2000. He has been at Leeds since 2006, initially as a Royal Society University Research Fellow and (since 2012) as a Professor of Satellite Geodesy. His work has been at the forefront of developing the use of satellite radar interferometry (InSAR) for measuring tectonic and volcanic deformation. His major achievements include the first demonstration that interseismic strain can be measured using InSAR, in this case for the North Anatolian Fault; the investigation of a series of major earthquakes using geodesy, seismology and geomorphology, including Bam (Iran, 2003), Denali (Alaska, 2002), and Izmit (Türkiye, 1999); the mapping and modeling of precursory inflation at a volcanic centre (Dabbahu, Ethiopia), and the subsequent discovery of a major rifting episode in Afar, Ethiopia. He has authored or coauthored more than 135 articles in major international journals, and his work is highly cited. He led the NERC-funded Afar Rift Consortium, a £3M project that is using a wide range of geophysical, geochemical and geologic techniques to investigate how the crust grows at divergent plate boundaries, and co-led LICS, an NERC large grant to "Look Inside the Continents from Space," which is producing open-access InSAR data over global volcanic and tectonic areas from sentinel-1.

Dr. Wright was the recipient of the William Smith Fund of the Geological Society in 2006, Philip Leverhulme Prize in 2014, Rosenstiel Award from the University of Miami, and AGU Geodesy Section Award, and in 2015. He was the British Geophysical Association's Bullerwell Lecturer. He was the Royal Astronomical Society's 2017 Harold Jeffreys Lecturer. He is the Director of the NERC Centre for the Observation and Modeling of Earthquakes, Volcanoes and Tectonics, and Co-Founder and Director of SatSense Ltd. Since 2023, he has been the Director of Research and Innovation with the School of Earth and Environment.

Andrew Hooper (Senior Member, IEEE) received the M.S. and Ph.D. degrees in geophysics from Stanford University, Stanford, CA, USA, in 2002 and 2006, respectively, for his development of SAR persistent scatterer interferometry algorithms for geophysical applications.

Between 2002 and 2003, he was with the German Space Center (DLR) on algorithms for the TerraSAR-X satellite. From 2006, he was with University of Iceland, before moving to Delft University of Technology in 2008. Since 2013, he has been a Professor of geophysics and geodesy with the University of Leeds, Leeds, U.K. His research interests include measuring and modeling deformation due to volcanic and tectonic processes, and the application of machine learning techniques to deformation data. Dr. Hooper was the recipient of the James B. Macelwane medal by the American Geophysical Union, given to outstanding early career scientists who have shown depth, breadth, impact, creativity and novelty in their research, in 2016. He is the Co-Founder and the Director of university spin-out SatSense.

Zahra Sadeghi received the M.S. and Ph.D. degrees in geomatics engineering-remote sensing, with a focus on developing performance of persistent scatterer InSAR techniques for crustal deformation mapping, from the K. N. Toosi University of Technology, Tehran, Iran, in 2011 and 2017, respectively.

As a part of her Ph.D. project from 2015 to 2017, she was a Visiting Researcher with the MSSL, University College London, U.K., and had a collaboration with the University of Leeds, Leeds, U.K., to present a novel polarimetric PSI method (PolStaMPS). After completing the Ph.D., she was with SatSense Ltd., Leeds, U.K., as an InSAR developer. In 2019, she was with COMET, School of Earth and Environment, University of Leeds, as a Postdoctoral Research Fellow. In this research position, she presented a new intercomparison method to ensure consistency between different InSAR datasets, and she also evaluated critical components of InSAR methods that impact infrastructural measurements. In 2022, she started a position with Spottitt Ltd., Harwell Science and Innovation Campus, Didcot, U.K., as a SAR/InSAR-Earth observation lead who is leading ground displacement analysis and infrastructures health monitoring projects using SAR imagery, InSAR, and machine learning techniques.

Sivasakthy Selvakumaran (Member, IEEE) received the B.A. and M.Eng. degrees in engineering and the Ph.D. degree in applied remote sensing from the University of Cambridge, Cambridge, U.K., in 2010 and 2019, respectively, and the C.Eng. degree with MICE professional engineering chartership qualifications from the Institution of Civil Engineers, London, U.K., in 2015.

She then worked in design, construction, and research and development roles within industries in Spain, Peru, and U.K. Her roles in industry included designing new structures on mega-projects like the Crossrail trainline in London, assessment to upgrade U.K., infrastructure assets, and working on sites to reconstruct housing destroyed by earthquakes. She has also worked in industry research and development roles for developing new solutions and technologies to change the way infrastructure is designed, constructed, and maintained. She spent part of her doctoral training as a Visiting Researcher with the German Aerospace Center, Oberpfaffenhofen, Germany, in 2019. She is the Isaac Newton Trust Fellow of engineering with the University of Cambridge. Her research focuses on the integration of remote sensing with structural monitoring to contribute toward sustainable and resilient cities.